

Cite this: *Chem. Sci.*, 2021, 12, 14414

All publication charges for this article have been paid for by the Royal Society of Chemistry

Molecular bixbyite-like In₁₂-oxo clusters with tunable functionalization sites for lithography patterning applications†

Xiaofeng Yi,^a Di Wang,^{ab} Fan Li,^{ab} Jian Zhang^{ID}^a and Lei Zhang^{ID}^{*a}

Indium oxides have been widely applied in many technological areas, but their utilization in lithography has not been developed. Herein, we illustrated a family of unprecedented In₁₂-oxo clusters with a general formula [In₁₂(μ₄-O)₄(μ₂-OH)₂(OCH₂CH₂NHCH₂CH₂O)₈(OR)₄X₄]X₂ (where X = Cl or Br; R = CH₃, C₆H₄NO₂ or C₆H₄F), which not only present the largest size record in the family of indium-oxo clusters (InOCs), but also feature the first molecular model of bixbyite-type In₂O₃. Moreover, through the labile coordination sites of the robust diethanolamine-stabilized In₁₂-oxo core, these InOCs can be accurately functionalized with different halides and alcohol or phenol derivatives, producing tunable solubility. Based on the high solution stability as confirmed by ESI-MS analysis, homogeneous films can be fabricated using these In₁₂-oxo clusters by the spin-coating method, which can be further used for electron beam lithography (EBL) patterning studies. Accordingly, the above structural regulations have significantly influenced their corresponding film quality and patterning performance, with bromide or *p*-nitrophenol functionalized In₁₂-oxo clusters displaying better performance of sub-50 nm lines. Thus, the here developed bixbyite-type In₁₂-oxo cluster starts the research on indium-based patterning materials and provides a new platform for future lithography radiation mechanism studies.

Received 16th August 2021

Accepted 19th September 2021

DOI: 10.1039/d1sc04491e

rsc.li/chemical-science

Introduction

Indium oxides (In₂O₃), existing in two phases of bixbyite- and corundum-type,¹ as n-type semiconductors possess unique electrical and optical properties with great prospects in extensive areas.^{2–7} For a better structure–property relationship understanding, it is essential to investigate In₂O₃ materials at the molecular level, for example indium-oxo clusters (InOCs) with a uniform row of structural fabrics and a clear chemical composition. Meanwhile, the exploration of InOCs also provides interesting opportunities for the development of new kinds of indium oxide materials with unprecedented functionalities. The frontier research realm of structurally well-defined InOCs was initiated by Wieghardt Karl and coworkers in 1986.⁸ In contrast to the remarkable progress in oxo clusters of transition metals^{9–11} and lanthanides,¹² the investigations on InOC chemistry were confined to structural archetypes including star, square, square-pyramid, octahedra, and wheel

geometry. And the largest size record in the family of InOCs has been limited to the In₁₀-oxo matrix to date,¹³ with even much less in developing their applications.¹⁴ Therefore, the consecutive exploration of InOCs is highly appealing to provide opportunities to enrich structural diversity and expand potential applications.

Nanoscale patterning enables ongoing miniaturization in dense integrated circuit technology to meet expectations predicted by Moore's law,^{15,16} and extreme ultraviolet (EUV) lithography as a promising next-generation lithography technology requires metal-containing patterning materials with large absorption cross-sectional characteristics for more efficient utilization of EUV photons.^{17–19} To date, a small number of metal complexes of Sn,^{20–23} Sb,²⁴ Hf,²⁵ Zr,²⁶ Ti,²⁷ Zn,²⁸ Pt and Pd²⁹ have set foot into this field. Interestingly, in terms of practical applications, the cage-like Sn-oxo cluster is exclusively available for realizing EUV lithography in industry, which indicate that metal-oxo clusters as a patterning material do have significant potential in nanolithography. It is absolutely imperative to facilitate the diversity and to study the radiation mechanism of such metal-containing patterning materials.

Considering the similar strong resonance towards EUV light of indium to the above heavy metals of Sn and Sb, In-based complexes are desperately expected to be promising patterning materials. In order to explore this possibility, InOCs can be an ideal research object for the following reasons: (1) InOCs possess an atomically precise structure favourable for

^aState Key Laboratory of Structural Chemistry, Fujian Institute of Research on the Structure of Matter, Chinese Academy of Sciences, Fuzhou, Fujian 350002, P. R. China. E-mail: LZhang@fjirsm.ac.cn

^bUniversity of Chinese Academy of Sciences, Beijing 100049, P. R. China

† Electronic supplementary information (ESI) available: Experimental details; additional figures and EBL patterns. CCDC 2078614–2078618 for InOC-1 to InOC-5. For ESI and crystallographic data in CIF or other electronic format see DOI: 10.1039/d1sc04491e

radiation mechanism study; (2) InOCs belong to molecular clusters with excellent solubility, which is conducive to film fabrication; (3) InOCs exhibit uniform distribution in size and composition, which can produce a homogeneous response during radiation; (4) the polynuclear characteristics of InOCs provide more utilization of shorter wavelength photons than mononuclear indium compounds; (5) InOCs can be accurately chemically modified by functionalizing with ligands for further optimization in patterning performance. Thus, research on InOC based patterning materials can fill the blank space of indium in this technologically important field, which might lay a foundation for future patterning materials with improved sensitivity, resolution and line edge roughness.

Results and discussion

Following the above consideration, herein we realized the assembly of In^{3+} ions with methanol or phenol derivatives under the assistance of diethanol amine as the stabilizing ligand into a series of novel In_{12} -oxo clusters $[\text{In}_{12}(\mu_4\text{-O})_4(\mu_2\text{-OH})_2(\text{OCH}_2\text{CH}_2\text{NHCH}_2\text{CH}_2\text{O})_8(\text{OR})_4\text{X}_4]\text{X}_2$ (where $\text{X} = \text{Cl}$, $\text{R} = \text{CH}_3$ for **InOC-1**; $\text{X} = \text{Br}$, $\text{R} = \text{CH}_3$ for **InOC-2**; $\text{X} = \text{Cl}$, $\text{R} = \text{C}_6\text{H}_4\text{NO}_2$ for **InOC-3**; $\text{X} = \text{Br}$, $\text{R} = \text{C}_6\text{H}_4\text{NO}_2$ for **InOC-4**; $\text{X} = \text{Cl}$, $\text{R} = \text{C}_6\text{H}_4\text{F}$ for **InOC-5**), whose patterning applications have been explored for the first time (Scheme 1). From the perspective of geometry, the obtained In_{12} -oxo clusters present the largest size record in the realm of InOCs. The In–O binding modes of the In_{12} core are analogous to those of bixbyite-type In_2O_3 , making them the first molecular models of bixbyite-type indium oxide. Meanwhile, there are 8 labile coordination sites in the robust In_{12} -oxo cluster to allow chemical decoration by various halides and functional alcohol or phenol derivatives. Moreover, these In_{12} -oxo clusters display good solubility and solution stability as confirmed by mass spectroscopy (MS), making them potential candidates for spin-coating nanofilm fabrication and further electron beam lithography (EBL) studies. Interestingly, the structural regulations on labile sites play important roles in their patterning applications, with *p*-nitrophenol or bromide decorated In_{12} -oxo-clusters showing high-performance patterning behaviors for excellent sub-50 nm pitch lines.

To synthesize crystalline indium-oxo clusters, it is crucial to decelerate the hydrolysis process of the In^{3+} ions for the improvement of crystallization. The recently developed and widely applied coordination delayed hydrolysis (CDH) strategy

was hence employed for the growth of InOC crystals.^{11,30} Diethanolamine was selected as the chelate initiator to protect In^{3+} ions from violent hydrolysis and also stabilize the produced In–O cores. Accordingly, the self-assembly of InCl_3 with diethanolamine in methanol at 100 °C for two days gave rise to block crystals of **InOC-1**.

Single-crystal X-ray structural analysis revealed that **InOC-1** represented a $\{\text{In}_{12}(\mu_4\text{-O})_4(\mu_2\text{-OH})_2\}$ core, which was further stabilized by eight diethanolamine $\text{NH}(\text{CH}_2\text{CH}_2\text{O})_2$ moieties accompanied by four chlorides and four functional organic segments OCH_3 (Fig. 1a). To the best of our knowledge, this In_{12} -oxo cluster has been the largest InOC reported to date. The 12 In^{3+} centers reside in the distorted octahedral coordination environment of $\text{In}_\alpha\{\text{InO}_6\}$, $\text{In}_\beta\{\text{InO}_5\text{Cl}\}$ and $\text{In}_\gamma\{\text{InO}_4\text{N}_2\}$, and then fused together by four $\mu_4\text{-O}$ and two $\mu_2\text{-OH}$ to form the $\text{In}_{12}\text{-O}$ core (Fig. S1 and S2†). The two $\mu_2\text{-OH}$ bridges in the $\text{In}_{12}\text{-oxo}$ skeleton are speculated by the bond valence sum calculation with a BVS value of *ca.* 1.0 (Table S6†) and recent studies showed that oxygen vacancies also play important roles in catalytic reactions.³¹ It is interesting to find that the planner- $\{\text{In}_6\}$ segments with rectangular geometry can serve as the basic building units, and there exist two such $\{\text{In}_6\}$ moieties parallel to each other and linked together *via* 4 $\mu_4\text{-O}$ to form the $\text{In}_{12}\text{-oxo}$ core (Fig. S2†). Furthermore, the In–O connectivity in this $\text{In}_{12}\text{-oxo}$ core is largely consistent with that in bixbyite-type In_2O_3 , making **InOC-1** the first ideal model of bixbyite-type In_2O_3 material at the molecular level (Fig. 2).

In the view of coordination chemistry, the four terminal chlorides in **InOC-1** should be quite labile to be replaced by other halides. Moreover, the four functional OCH_3 segments could also be modified with their alcohol or phenol derivatives.

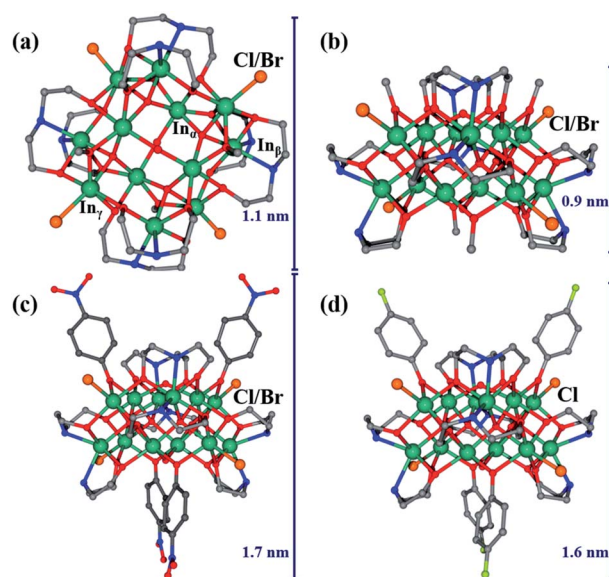
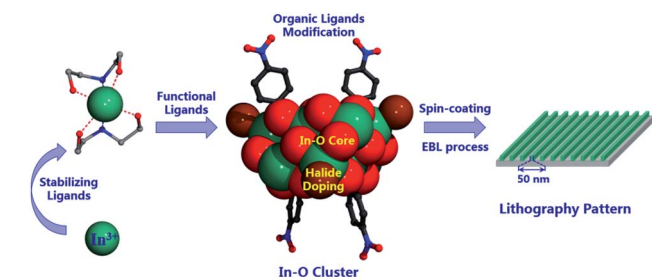


Fig. 1 (a) Molecular structure of **InOC-1** and **InOC-2** in top views. (b) Molecular structure of **InOC-1** and **InOC-2** in side views. (c) Molecular structure of **InOC-3** and **InOC-4** in side views. (d) Molecular structure of **InOC-5** in side views. Atom color code: dark-green, In; red, O; blue, N; gray, C; orange, Cl or Br; lime, F. All H atoms have been omitted for clarity.



Scheme 1 Illustration of the assembly of the atomically precise In_{12} -oxo clusters with chemical modification and patterning evaluation.



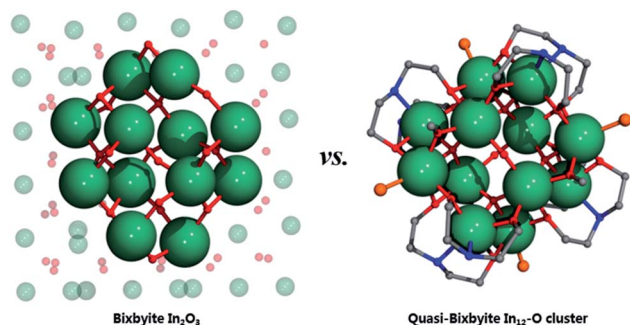


Fig. 2 Contrastive illustration of In–O connectivity in the bixbyite In_2O_3 (left) and the In_{12} -oxo skeleton (right) of **InOC-1**. Atom color code: dark-green, In; red, O; blue, N; gray, C; orange, Cl. All H atoms have been omitted for clarity.

Therefore, there are 8 possible labile sites on the In_{12} -core in total for further structural functionalization on **InOC-1**. Indeed, when InBr_3 was applied instead of InCl_3 , bromide functionalized **InOC-2** was obtained. It displays the same In_{12} -core as **InOC-1** except for the four terminating bromide ions (Fig. S4†). To verify the modification ability on OCH_3 sites, methanol in the synthesis of **InOC-1** was replaced by *p*-nitrophenol and tetrahydrofuran (THF) as the organic ligand and solvent, respectively, leading to the formation of **InOC-3**. As shown in Fig. 1c and S5,† four *p*-nitrophenol segments were successfully introduced into **InOC-3** as the substitute of the four OCH_3 in **InOC-1**. The versatility of these labile sites was further confirmed by the construction of **InOC-4** and **InOC-5** with $-\text{Br}/-p$ -nitrophenol and $-\text{Cl}/-p$ -fluorophenol as chemical modification on the In_{12} -core, respectively (Fig. S6 and S7†). These cationic In_{12} -oxo clusters in **InOC-1** to **InOC-5** display square configuration with similar side lengths of *ca.* 1.1 nm but different thicknesses (maximum extension of the organic groups OR) ranging from *ca.* 0.9 to 1.7 nm.

It is known that subtle fluctuations in the material structures or composition dominate their electronic structure and the Hansen solubility parameters (HSPs).^{19,32} Therefore, we intended to probe the In_{12} -oxo core as a platform for the comparative exploration of their photophysical characteristics as well as HSP values related to solution behaviors. Verified by powder X-ray diffraction analysis (Fig. S13 to S17†), **InOC-1** to **InOC-5** in the solid state are in a highly pure phase allowing for further inspection. Solution experiments indicated that **InOC-1** to **InOC-5** could be readily dissolved in dimethyl formamide (DMF). Among them, **InOC-1** exhibits relatively poor solubility, which could be improved by ultrasonic treatment and increasing the dissolution time. It is interesting that the implantation of bromide in place of chloride increases the solubility of **InOC-2** in DMF. More importantly, the introduction of strong electron withdrawing ligands *p*-nitrophenol or *p*-fluorophenol instead of methanol into the In_{12} -oxo backbone endows **InOC-3** to **InOC-5** with much higher solubility in DMF. Thus, $-\text{Br}/-p$ -nitrophenol decorated **InOC-4** presents the highest solubility among these In_{12} -oxo clusters. Then electrospray ionization mass spectrometry (ESI-MS) analysis was applied to

investigate the stability of the In_{12} -oxo clusters after dissolution. As shown in Fig. 3, the positive ion mode ESI spectrum of **InOC-1** in DMF exhibits a unique isotope envelope from *m/z* 1250 to 1275 of +2 charged species. In comparison of the experimental and simulated patterns, these +2 charged species could be attributed to $\{\text{In}_{12}\text{-cluster}\}^{2+}$ ions based on the intact $[\text{In}_{12}(\mu_4\text{-O})_4(\mu_2\text{-OH})_2(\text{dea})_8(\text{OR})_4\text{Cl}_4]^{2+}$ ($\text{dea} = \text{OCH}_2\text{CH}_2\text{NHCH}_2\text{CH}_2\text{O}$) species missing halides or organic OCH_3 groups (Table S11†). Furthermore, $\{\text{In}_{12}\text{-cluster}\}$ related species are capable of aggregation into a small number of +3 charged dimers in the *m/z* range between 1680 and 1710. In addition, the In_{12} -oxo clusters dissolved in DMF can be extracted with the assistance of propylene glycol methyl ether acetate (PGMEA), whose FT-IR spectra were in good agreement with those of original **InOC-1** to **InOC-5** (Fig. 3c and S33 to S36†). Therefore, the MS measurements and FT-IR measurements evidenced the high

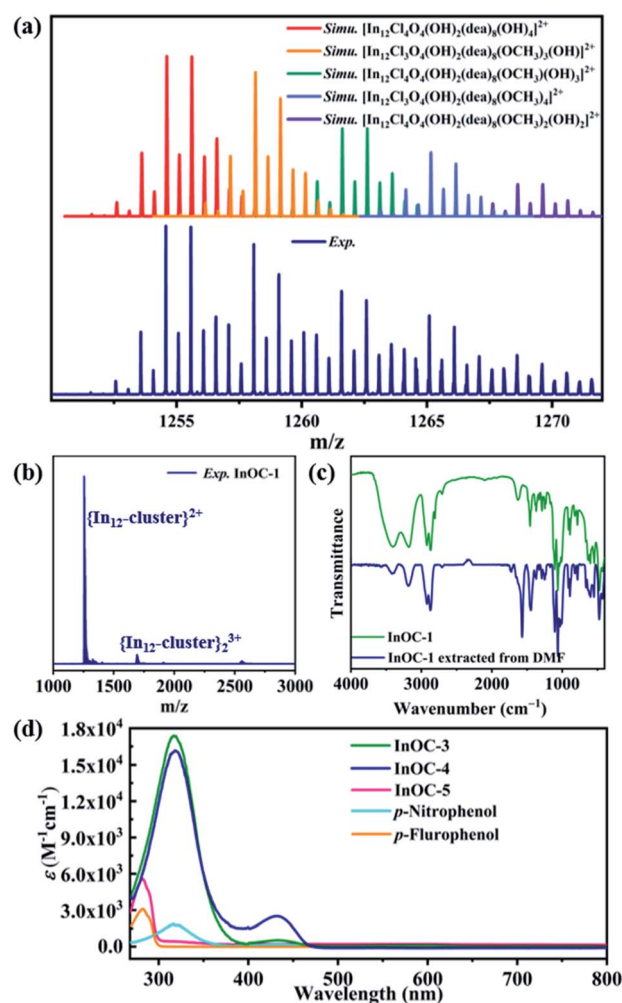


Fig. 3 (a) The comparison of the experimental isotopic envelope with simulated patterns of the predominant species of $\{\text{In}_{12}\text{-cluster}\}^{2+}$ and (b) positive-mode ESI-MS entire spectrum of **InOC-1** in DMF; (c) comparison of the FT-IR spectra of **InOC-1** (olive) and **InOC-1** dissolved in DMF followed by extraction with the assistance of PGMEA (navy); (d) comparative UV-Vis spectra of **InOC-3**, **InOC-4**, **InOC-5** and their corresponding free ligands *p*-nitrophenol and *p*-fluorophenol in DMF.

solution stability of these In_{12} -oxo clusters in the DMF medium. Moreover, the observed aggregation behaviors through their interaction with energetic electrons during the ionization process further support the prospects for their application as patterning materials.

Besides solubility, the functionalized ligands on In_{12} -oxo cores also influence their photophysical properties, as confirmed by solution UV-Vis absorption spectroscopy studies (Fig. 3d). The absorption of colorless **InOC-1** and **InOC-2** in DMF was almost negligible in the range of 268 to 800 cm^{-1} . Meanwhile the introduction of strong electron withdrawing ligands *p*-nitrophenol or *p*-fluorophenol endows the In_{12} -oxo clusters with obvious absorption peaks. Among them, *p*-nitrophenol decorated **InOC-3** or **InOC-4** shows a greater absorption coefficient and more significant red-shift adsorption (at 316 nm, $\epsilon = 17\,349\text{ L cm}^{-1}\text{ mol}^{-1}$ for **InOC-3**; at 316 nm, $\epsilon = 16\,043\text{ L cm}^{-1}\text{ mol}^{-1}$ for **InOC-4**) than *p*-fluorophenol decorated **InOC-5** (at 282 nm, $\epsilon = 5570\text{ L cm}^{-1}\text{ mol}^{-1}$). More interestingly, the absorption of yellowish **InOC-3** and **InOC-4** modified with *p*-nitrophenol can occur in the visible light region, which is consistent with its appearance color. Furthermore, the absorption maxima position in the spectra of **InOC-3** to **InOC-5** could be compared with the spectral characteristics of free *p*-nitrophenol or *p*-fluorophenol, but they exhibit a much larger absorption coefficient than their corresponding free decorated ligands. Among them, the yellowish **InOC-3** and **InOC-4** decorated with four *p*-nitrophenol ligands display a much larger 4 times higher absorption coefficient than free *p*-nitrophenol.

In combination with the above structural and solubility analysis, the obtained In_{12} -oxo clusters can provide molecular

candidates for smooth film formation, which might be used as In-containing patterning materials (Fig. 4a). Furthermore, the sophisticated functionalization on the In_{12} -oxo platform with different halides and organic species with various electron-withdrawing groups may influence their film quality and patterning performance, providing unprecedented opportunities to understand the relationship between the chemical modification on In–O cores and their radiolysis attributes. To this end, the patterning performance differences among **InOC-1** to **InOC-3** have been evaluated by electron beam lithography (EBL), which can produce high-energy electrons during radiation interaction to induce chemical changes in materials for pattern formation. The quite poor solubility of inorganic bixbyite- In_2O_3 particles usually results in heterogeneous films, preventing further patterning evaluation. In contrast, it is very interesting that clear patterns have been fabricated under electron-beam exposure using these three In_{12} -oxo clusters, which is firstly found for indium-based materials. As shown in Fig. 4 and S43,† **InOC-1** with the decoration of chloride and methoxy demonstrated 1 : 2 line-to-space patterns with feature sizes from 1000 to 100 nm under a dose of 1000 $\mu\text{C cm}^{-2}$, which are unfortunately not uniform and present low contrast. In contrary, the electron beam lithographic performance of **InOC-2** and **InOC-3** based patterning materials was significantly improved with homogeneous lines observed, and there were not any bridging problems or residues observed in the unexposed areas. This might be due to the improved solubility of **InOC-2** and **InOC-3** compared to **InOC-1**, giving rise to more homogeneous films with higher quality (Fig. S42†) and better patterns. More importantly, smaller critical dimensions of 50 nm were printed upon radiation with a dose of 1000 $\mu\text{C cm}^{-2}$ for **InOC-2** and **InOC-3**, as evidenced by scanning electron microscopy (SEM) images (Fig. S44e and S45e†). For **InOC-3**, atomic force microscopy (AFM) studies indicated that satisfactory 50 nm lines could even be fabricated under a lower radiation energy of 500 $\mu\text{C cm}^{-2}$ (Fig. 4f). Therefore, these results support a speculated radiolysis process, where the halide and organic ligand sites of the In_{12} -oxo clusters involved in changing the film dissolution behaviors after the EBL treatment. The introduction of bromide instead of chloride, especially *p*-nitrophenol instead of methoxy, can significantly increase the sensibility of In_{12} -oxo cluster based films upon EBL radiation to produce better patterns. These findings suggest that bixbyite-like In_{12} -oxo clusters not only present competitive advantages in nanolithography, but also may provide a platform for understanding structure–property (*e.g.* solubility, film quality and patterning ability) relationships in indium oxide materials at the molecular level.

Conclusions

In summary, we successfully isolated and characterized a series of atomically precise In_{12} -oxo clusters from the self-assembly of InX_3 ($\text{X} = \text{Cl}$ or Br) with diethanolamine as the chelate initiator. In terms of the structure, these In_{12} -oxo clusters not only record the largest size in the family of InOCs but also elucidate the first molecular model of bixbyite-type indium oxide. The robust

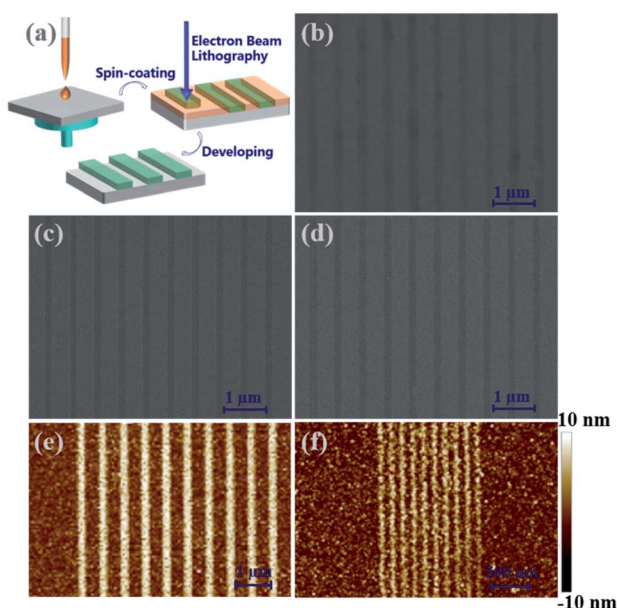


Fig. 4 (a) Schematic illustration of the patterning process of In_{12} -oxo clusters. SEM images of patterns with 200 nm lines obtained using electron-beam lithography performed with a dose of 1000 $\mu\text{C cm}^{-2}$ for **InOC-1** (b), **InOC-2** (c) and **InOC-3** (d). AFM images of patterns obtained with a dose of 500 $\mu\text{C cm}^{-2}$ exhibiting feature sizes of 200 nm (e) and 50 nm (f) for **InOC-3**.



diethanolamine-stabilized In₁₂-oxo core presents 8 labile sites on the cluster surface, which allow chemical modification with various terminating halides and bridging methoxy or phenyl derivatives. In addition, such cluster functionalization further leads to variable solubility in DMF, and the solution stability of these In₁₂-oxo clusters has been confirmed by ESI-MS studies. Moreover, their patterning performance was evaluated under the exposure of an electron beam, which is of particular interest because indium-based patterning materials for lithography have never been studied before. Among them, compared to chloride and methoxy functionalized InOC-1, InOC-2 and InOC-3 with bromide or *p*-nitrophenol moieties exhibited better patterning performance with a feature size of 50 nm lines. Therefore, this work not only provides an interesting In₁₂-oxo model for bixbyite-type indium oxide, but also opens the patterning applications of indium-based materials whose performance can be improved through chemical structure modification.

Data availability

The datasets supporting this article have been uploaded as part of the ESI.†

Author contributions

L. Z. designed the study and supervised the project; X. Y. implemented materials synthesis and characterization; X. Y and D. W. carried out electron-beam lithography studies; F. L. assisted materials characterization. All authors discussed the results and co-wrote the manuscript.

Conflicts of interest

There are no conflicts to declare.

Acknowledgements

The research reported in this publication was supported by the National Natural Science Foundation of China (21922111, 91961108, and 21901241), the Strategic Priority Research Program of the Chinese Academy of Sciences (XDB20000000), and the Natural Science Foundation of Fujian Province (2020J01117). We appreciate Lv-Bing Yuan for assisting in single-crystal XRD data collection, Ling-Ling Zheng for SEM measurements, Dan-Mei Pan for AFM measurements, and Prof. Li Xu for providing synthetic assistance.

Notes and references

- 1 M. Marezio, *Acta Crystallogr.*, 1966, **20**, 723–728.
- 2 T. Li, Z. Chen, Y. Wang, J. Tu, X. Deng, Q. Li and Z. Li, *ACS Appl. Mater. Interfaces*, 2020, **12**, 3301–3326.
- 3 S. Li, M. Tian, Q. Gao, M. Wang, T. Li, Q. Hu, X. Li and Y. Wu, *Nat. Mater.*, 2019, **18**, 1091–1097.
- 4 L. Wang, Y. Dong, T. Yan, Z. Hu, A. A. Jelle, D. M. Meira, P. N. Duchesne, J. Y. Y. Loh, C. Qiu, E. E. Storey, Y. Xu, W. Sun, M. Ghoussoub, N. P. Kherani, A. S. Helmy and G. A. Ozin, *Nat. Commun.*, 2020, **11**, 2432.
- 5 Y. Qi, L. Song, S. Ouyang, X. Liang, S. Ning, Q. Zhang and J. Ye, *Adv. Mater.*, 2019, 1903915, DOI: 10.1002/adma.201903915.
- 6 Y. X. Pan, Y. You, S. Xin, Y. Li, G. Fu, Z. Cui, Y. L. Men, F. F. Cao, S. H. Yu and J. B. Goodenough, *J. Am. Chem. Soc.*, 2017, **139**, 4123–4129.
- 7 H. Yan, K. He, I. A. Samek, D. Jing, M. G. Nanda, P. C. Stair and J. M. Notestein, *Science*, 2021, **371**, 1257–1260.
- 8 K. Wieghardt, M. Kleine-Boymann, B. Nuber and J. Weiss, *Inorg. Chem.*, 1986, **25**, 1654–1659.
- 9 Advances in Inorganic Chemistry, *Polyoxometalate Chemistry*, ed. R. van Eldik and L. Cronin, Zee Kruze, 1st edn, 2017.
- 10 P. Yang and U. Kortz, *Acc. Chem. Res.*, 2018, **51**, 1599–1608.
- 11 W. H. Fang, L. Zhang and J. Zhang, *Chem. Soc. Rev.*, 2018, **47**, 404–421.
- 12 X. Y. Zheng, Y. H. Jiang, G. L. Zhuang, D. P. Liu, H. G. Liao, X. J. Kong, L. S. Long and L. S. Zheng, *J. Am. Chem. Soc.*, 2017, **139**, 18178–18181.
- 13 N. N. Chamazi, M. M. Heravi and B. Neumüller, *Z. Anorg. Allg. Chem.*, 2006, **632**, 2043–2048.
- 14 Z. L. Mensinger, W. Wang, D. A. Keszler and D. W. Johnson, *Chem. Soc. Rev.*, 2012, **41**, 1019–1030.
- 15 A. Robinson, *Frontiers of Nanoscience Materials and Processes for Next Generation Lithography*, Elsevier, 2016.
- 16 M. Tu, B. Xia, D. E. Kravchenko, M. L. Tietze, A. J. Cruz, I. Stassen, T. Hauffman, J. Teyssandier, S. De Feyter, Z. Wang, R. A. Fischer, B. Marmiroli, H. Amenitsch, A. Torvisco, M. J. Velasquez-Hernandez, P. Falcato and R. Ameloot, *Nat. Mater.*, 2021, **20**, 93–99.
- 17 L. Li, X. Liu, S. Pal, S. Wang, C. K. Ober and E. P. Giannelis, *Chem. Soc. Rev.*, 2017, **46**, 4855–4866.
- 18 N. Mojarad, M. Hojeij, L. Wang, J. Gobrecht and Y. Ekinici, *Nanoscale*, 2015, **7**, 4031–4037.
- 19 P. D. Ashby, D. L. Olynick, D. F. Ogletree and P. P. Naulleau, *Adv. Mater.*, 2015, **27**, 5813–5819.
- 20 B. Cardineau, R. Del Re, M. Marnell, H. Al-Mashat, M. Vockenhuber, Y. Ekinici, C. Sarma, D. A. Freedman and R. L. Brainard, *Microelectron. Eng.*, 2014, **127**, 44–50.
- 21 J. T. Diulus, R. T. Frederick, D. C. Hutchison, I. Lyubnitsky, R. Addou, M. Nyman and G. S. Herman, *ACS Appl. Nano Mater.*, 2020, **3**, 2266–2277.
- 22 S. Saha, D. H. Park, D. C. Hutchison, M. R. Olsen, L. N. Zakharov, D. Marsh, S. Goberna-Ferron, R. T. Frederick, J. T. Diulus, N. Kenane, G. S. Herman, D. W. Johnson, D. A. Keszler and M. Nyman, *Angew. Chem., Int. Ed.*, 2017, **56**, 10140–10144.
- 23 I. Bepalov, Y. Zhang, J. Haitjema, R. M. Tromp, S. J. van der Molen, A. M. Brouwer, J. Jobst and S. Castellanos, *ACS Appl. Mater. Interfaces*, 2020, **12**, 9881–9889.
- 24 J. Passarelli, M. Murphy, R. D. Re, M. Sortland, J. Hotalen, L. Dousharm, R. Fallica, Y. Ekinici, M. Neisser, D. A. Freedman and R. L. Brainard, *J. Micro/Nanolithogr., MEMS, MOEMS*, 2015, 14.



- 25 J. Jiang, S. Chakrabarty, M. Yu and C. K. Ober, *J. Photopolym. Sci. Technol.*, 2014, **27**, 663–666.
- 26 G. Kickelbick, P. Wiede and U. Schubert, *Inorg. Chim. Acta*, 1999, **284**, 1–7.
- 27 L. Wu, M. Tiekink, A. Giuliani, L. Nahon and S. Castellanos, *J. Mater. Chem. C*, 2019, **7**, 33–37.
- 28 H. Xu, K. Sakai, K. Kasahara, V. Kosma, K. Yang, H. C. Herbol, J. Odent, P. Clancy, E. P. Giannelis and C. K. Ober, *Chem. Mater.*, 2018, **30**, 4124–4133.
- 29 O. R. Wood, E. M. Panning, M. Sortland, R. Del Re, J. Passarelli, J. Hotalen, M. Vockenhuber, Y. Ekinici, M. Neisser, D. Freedman and R. L. Brainard, *Extreme Ultraviolet (EUV) Lithography VI*, 2015, DOI: 10.1117/12.2086598.
- 30 D. Wang, Z.-N. Chen, Q.-R. Ding, C.-C. Feng, S.-T. Wang, W. Zhuang and L. Zhang, *CCS Chemistry*, 2020, 2607–2616, DOI: 10.31635/ccschem.020.202000546.
- 31 A. Tsoukalou, P. M. Abdala, D. Stoian, X. Huang, M. G. Willinger, A. Fedorov and C. R. Muller, *J. Am. Chem. Soc.*, 2019, **141**, 13497–13505.
- 32 M. Larsen, *Proceedings of the 17th International Conference on Composite Materials ICCM-17*, 2009.

